3.1 Structure of Vortex Breakdown on a Delta Wing

The two basic phenomena that characterise flow over a delta wing are the formation of leading edge vortices and their breakdown at high incidence. While the vortex induced suction generates additional lift, vortex breakdown causes loss of lift on the aft part of the wing, resulting in a nose up pitching moment, a rolling moment, buffetting and poor control. Vortex breakdown is characterised by a sudden drop in the vortex suction and a large change in the vortex core velocity field.

While earlier studies, in spite of using very fine grids, have only given a broad picture of these interesting and important flow fields, none has so far yielded the kind of fine structure considered here. The present work employs a new type of grid, called the embedded conical grid, which exploits the special nature of the flow field necessary to obtain a well resolved vortex structure right from the apex.

Numerical investigation of vortex breakdown phenomenon on a 70 deg. sharp-edged delta wing at 30 deg. incidence in a subsonic free-stream has been carried out. Fig. 3.1 shows a numerical flow visualisation of breakdown where sudden belling out of the near-axis streamlines can be seen.

The breakdown process was observed to begin at the vortex axis as a sudden rapid deceleration of the inner core due to a sudden increase in the adverse axial pressure gradient. This vigorously

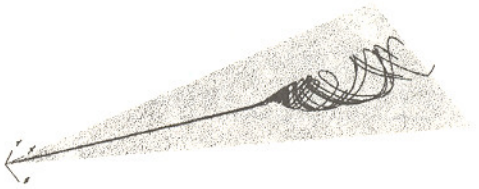

Fig. 3.1: Near-axis streamlines showing sudden broadening of the vortex core due to breakdown on a 70 deg delta wing at free-stream Mach number of 0.3 and incidence of 30 deg

pushes the surrounding fluid outward, causing a sudden broadening of the core and a significant reduction in the magnitude of the azimuthal velocity in the inner core. Streamlines through the conically projected velocity field in the normal planes just upstream of, at and just after the breakdown are displayed in Fig. 3.2 which show that the near-axis flow changes from conically inward to conically outward. The rapid deceleration of the inner core further leads to the formation of a deficit velocity region around the vortex axis, which builds up rapidly and leads to axial flow reversal.

A significant reduction in the magnitude of the axial vorticity takes place during the breakdown. The near-axis vorticity lines which are co-rotating with the flow upstream of the breakdown, were found to suddenly tilt away from the axis at breakdown and their spiralling direction was reversed, i.e., the azimuthal vorticity becomes negative. *(A. Kumar)*

3.2 Shock-induced Secondary Vortex on a Delta Wing

On a sharp-edged delta wing placed in a transonic free-stream the flow separates from the wing leading-edges forming the primary vortices. As the incidence is increased the outboard flow beneath the primary vortex can attain supersonic speeds. This flow, which is highly spanwise, must turn to align itself with the wind-side flow at the leading-edge. Under appropriate conditions, this may lead to the formation of a cross-flow shock, and a shock-induced secondary separation, leading to the formation of a secondary vortex.

Earlier Euler simulations of transonic flow over delta wings, in spite of using very fine grids, have not shown the shock-induced secondary vortices. The present investigation has shown that this results from an inherent deficiency of the computational grids employed. By employing the embedded conical grid that correctly takes into account the length scales of the flow, for the first time, a lee-side flow, containing embedded cross-flow shocks and shock-induced secondary vortices, is obtained, right from the apex of the wing. The computed lee-surface flow pattern and the experimental (Houtman and Bannink, TU Delft Report LR-518, 1987) surface oil-flow visualisation are compared in Fig. 3.3. *(A. Kumar)*

3.3 Motion of a Sphere in an Inhomogeneous Viscous Fluid

Certain polymers show the following interesting phenomenon. When a sphere is dropped in the fluid, it leaves behind a 'depleted region'. Subsequently when another sphere is dropped, its motion drifts towards the axis of the motion of the first sphere. This phenomenon has remained unexplained. Numerical simulations have been carried out in two-dimension (a cylinder in a channel) and in three- dimension (a sphere in a cylinder) to explain the phenomenon through a viscosity stratification which may arise due to

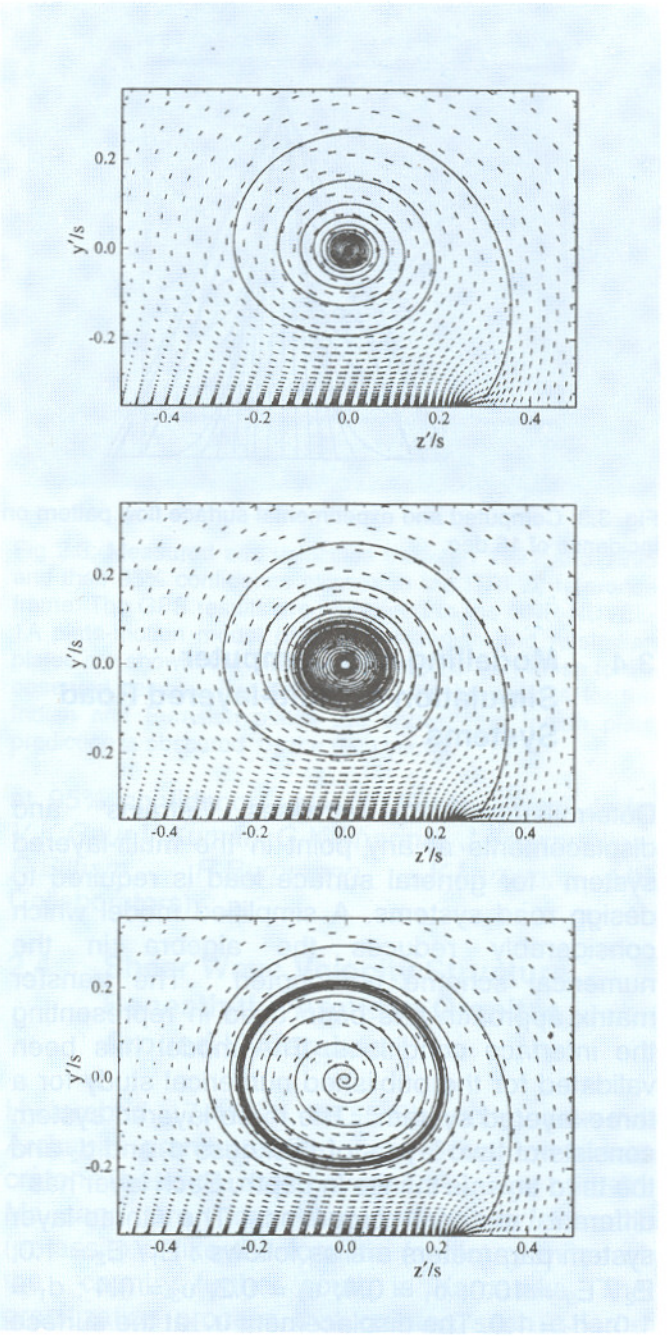

Fig. 3.2: Streamlines through the conically projected velocity field in the normal planes just upstream, at and just downstream of the breakdown showing the changes in the near axis flow due to the breakdown.

breakage of hydrogen-bonding. *(A. Kumar, R. A. Mashelkar*, *CSIR, New Delhi)*

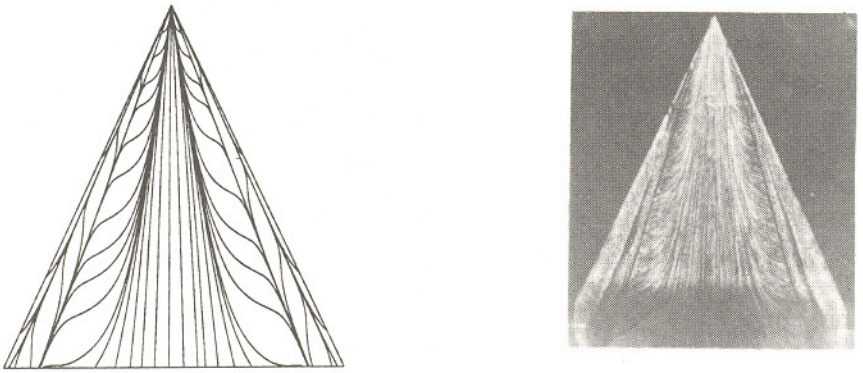

Fig. 3.3: Computed and experimental surface flow pattern on a 65 deg delta wing at free-stream Mach number of 0.85 and incidence of 15 deg.

3.4 Modelling and Computer Simulation of Multi-layered Road Systems

Determination of stresses, strains and displacements at any point in the multi-layered system for general surface load is required to design road systems. A simplified model which considerably reduces the algebra in the numerical scheme is adopted. The transfer matrix approach has been used in representing the interface conditions. The model has been validated for the published numerical study for a three-layered system. The three-layered system consists of two layers of thickness d_1 and d_2 and the third layer is infinite in depth. Each layer has different material propeties. The three-layer system parameters are as follows : $E_1 / E_2 = 1.0$; $E_2 / E_3 = 10.0$; $\upsilon_1 = 0.4$; $\upsilon_2 = 0.2$; $\upsilon_3 = 0.4$; $d_1 = 1.0$; $d_2 = 1.0$. The displacement u_z at the surface beneath the centre of the uniformly loaded circular area of radius 'a' , and the intensity of the load 'P' has been determined for different values of 'a'. The comparison of the results obtained by the present analysis and the numerical results given by Sciffman are presented in Table 3.1.

The model (and the software) can take care of any number of layers for analysis, and the values of stresses, strains and displacements can be determined at any point in the n-layered medium, for both the uniformly distributed and concentrated surface loads. The comparison of the model results with the Falling Weight Deflection (FWD) field data is in progress.

Preparation of database on pavement surface deflection of some existing roads and determination of *E*-values for different component layers for a three-layered pavement structure for different levels of stress using a ELMOD software have been completed. An experimental pavement section was prepared in the campus of CRRI for testing under controlled conditions. FWD data has been generated over a wide range of wheel loads. Data has also been collected for different environmental conditions on a few typical road sections and the results are being analysed. Detailed analysis of FWD data is being carried out for determining the material properties of different pavement component layers. *(Sridevi Jade, P.K. Nanda*, K.K. Verma*, S.P. Pokhriyal*, *CRRI, New Delhi)*

a- radius of the uniformly loaded area	u_z / pa × 10^{-5}	
	Sciffman	Present model
0.4	0.14773	0.14253
0.6	0.18007	0.17665
0.8	0.21143	0.21072
1.0	0.24220	0.24085
1.5	0.31565	0.31430
2.0	0.38283	0.38148
3.0	0.49574	0.49431
4.0	0.58157	0.58023
5.0	0.64511	0.64377
6.0	0.69142	0.69009

Table 3.1: Comparison of settlement surface u_z for a three-layered medium

3.5 Finite Element Analysis of Reinforced Earth Wall

Two-dimensional finite element analysis of a reinforced earth retaining wall has been carried out and the results are compared with the actual field performance. The reinforced earth retaining wall, 33m in length and 1.59m in height, was built to replace the conventional brick masonry retaining wall in the CBRI campus. The precast reinforced brick facing panels of the retaining wall and the backfill material has been modelled using 2-D four node isoparametric plane strain quadrilateral element. The reinforcing element has been modeled as two-dimensional line element. The interface between the reinforcing material and the soil has been modelled using interface element which may maintain or break physical contact and may slide relative to each other. The element is capable of supporting only compression in the direction normal to the surface and shear (Coulomb friction) in the tangential direction. The element is non-linear and may have an open or closed status The element is defined by two-nodal points, an interface angle, stiffness K, coefficient of friction, an initial displacement interference and an initial element status. The element is represented by a pair of coupled nonlinear orthogonal springs in normal and tangential directions to the interface and requires an iterative solution for static convergence procedure. The element is assumed to have converged when its status doesn't change between two successive iterations. However in cases of frictional contact, the element oscillates between sliding and sticking status, then the convergence criteria on the shear force has to be satisfied.

The FEM analysis has been carried out for the self weight of the retaining wall system. The nonlinearity considered in the analysis is geometric nonlinearity introduced by the interface element in the form of boundary nonlinearity. All the other elements remain linear elastic throughout the analysis. In the case of geometric nonlinearity the classical theory of infinitesimal strains doesn't hold and the strains are obtained from the displacements via a nonlinear operator. This type of nonlinearity may involve large displacements, rotations and finite strains. Since geometric nonlinearity is considered the force convergence criterion is used.

The stress field, lateral displacement of the retaining wall and vertical settlement of the backfill earth have been determined for different stiffness values and also by varying the Young's modulus E value of the soil. The predicted vertical settlement of the backfill is compared with the observed settlement in the field (Fig. 3.4). *(Sridevi Jade, K.G.Garg*, *CBRI, Roorkee)*

3.6 Behaviour of Masonry Infilled R.C.C. Frames

Composite action between the bounding R.C.C. frame and the infilling wall of brick masonry, which alters the frame characteristics, has been a subject of study for nearly four decades. Analysis of composite wall-beam systems have been attempted with varying degrees of sophistication. The computational task has restricted the detailed stress analysis of the problem. The limitations of the techniques have also precluded consideration of physical separation which tends to occur between the wall and beam/column - an important factor in the total behaviour. Now with the availability of high performance computing and the finite element method of stress analysis, it is possible

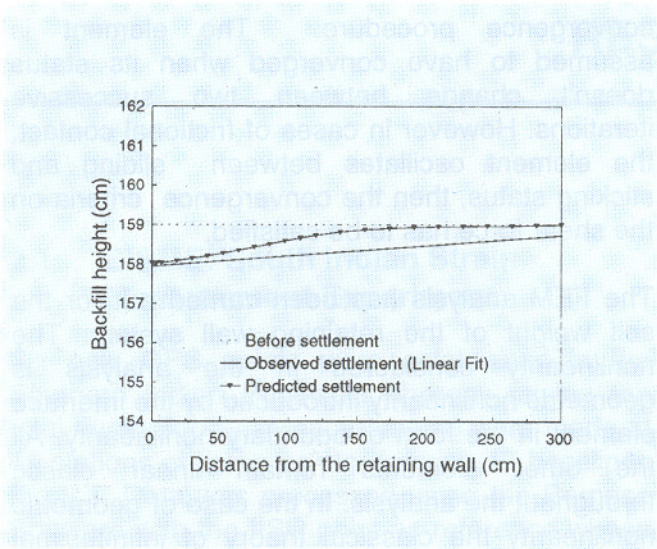

Fig.3.4: Vertical settlement profile of the topmost surface of the earth backfill of the wall.

to analyse such highly indeterminate structures with ease.

The structural parameters which influence interaction are the beam stiffness, physical separation at the interface and number of storeys. The support condition of the plinth beam (either fully supported or unsupported) influences the behaviour of the frame, as plinth beams does not rest on rigid base, but on flexible elastic foundation. The actions which relate particularly to arching and which must be considered in developing a design method are the bending moments, tie forces and deflections in the r.c. elements and stresses in walls. Absence of ground floor wall, which is common in multi-storeyed structures (to provide for parking space and other amenities) also affects interaction.

The idealised masonry infilled frame structure used for the analysis comprises of a wall of linear elastic homogeneous material, to represent brickwork, enclosed in a r.c. elastic frame. The masonry is represented by 2-D four-noded rectangular plane stress elements and r.c. members are represented by 3-D beam elements. The interface between them is represented by short, very stiff beam elements. This arrangement helps in establishing the `length of contact' of arching action during transfer of loads. All the parameters which affect interaction (discussed above) are considered and the results are compared with plane frames using conventional method of analysis (without considering interaction).

The results show that arching action in masonry reduces the bending moments and deflections significantly. Shear forces and axial forces in the beams and columns are also reduced. However, axial forces in the beams are to be taken into account during their design. Design of r.c. elements in the frame using the above analysis is highly economical, besides rational. The wall stresses are also reduced when interaction is taken into account, though there are areas of stress-concentration near beam-column junctions. A typical principal stress contour for a two-storeyed infilled frame subjected to normal vertical loading is shown in Fig. 3.5.

Thus there are two important points to be considered during the construction of the wall to avail the advantage of interaction. If a wall is built on a propped beam, as construction proceeds, the weight of unset wall will be distributed over the length of the beam, thus preventing the wall load from arching. Therefore, the beam should be propped during construction until the wall is cured. Secondly, the walls which are assumed to act compositely with frame elements, must be declared as structural elements and they should not be allowed to be removed or openings created in them at a later stage *(Sridevi Jade, V. Ramachandra*, R. Jagadish*, *B'lore Univ.).*

3.7 Strength Contours of Leather Surfaces

A collaborative project between C-MMACS and CLRI was initiated for developing software tools that would facilitate optimizing the use of leather.

About 332 test samples were cut perpendicular to the direction of backbone according to Bureau of Indian Standards (BIS) from Chrome tanned

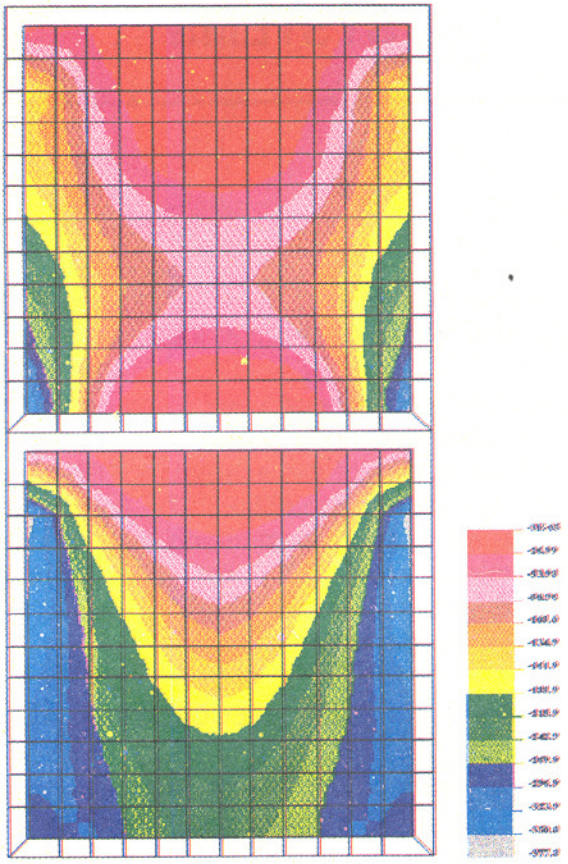

Fig. 3.5: Principal stress contours in a two-storeyed masonry infilled R.C.C. frame.

cow upper crust for the measurement of tensile strength and elongation at break. The software package developed at C-MMACS was used to visualize the strength profile of cow hide in the form of 3-D colour contour with a view to

Fig. 3.6: Strength profile of cow hide

understand the variation in strength at different locations (Fig. 3.6).

In addition, the existing software package was modified to calculate the area occupied by various colours in the colour contour mapping in the 3-D strength profile and the percent area occupied by each colour which can help the leather product industries about the useful portion of the skin. Efforts are being made to get multiple data at the same point of the leather sample. *(M.K.Sharada, B. Lokanadam*, *CLRI, Madras)*